

Article

Compression-Induced Dehydrogenation of Graphene: Insight from Simulations

Danil W. Boukhvalov ^{1,2,*}  and Vladimir Yu. Osipov ³ 

¹ Institute of Materials Physics and Chemistry, College of Science, Nanjing Forestry University, Nanjing 210037, China

² Institute of Physics and Technology, Satbayev University, Alma Ata A25A1G8, Kazakhstan

³ Ioffe Institute, Polytechnicheskaya 26, St. Petersburg 194021, Russia; osipov@mail.ioffe.ru

* Correspondence: danil@njfu.edu.cn

Abstract: In this work, we reported the results of systematic studies of various configurations of chemically adsorbed hydrogen atoms on the surface of corrugated graphene induced by in-plane uniaxial compression. Different magnitudes of the substrate corrugations have been considered. Results of the calculations demonstrate the visible difference in the electronic structure of corrugated non-hydrogenated graphene, contrary to the absence of a visible effect of corrugation of graphene. The reciprocal effect of corrugation and local hydrogenation on the permeation of protons (H⁺) throughout the graphene membrane is also discussed. Results of the periodic DFT calculations demonstrate that binding energy between graphene and large hydrogen clusters drastically decreases with increasing the magnitudes of the corrugation graphene substrate. A similar effect of decreasing hydrogen binding energies was also observed for corrugated graphane. The obtained results can be used to control the release of hydrogen from graphene by switching mechanical stress on and off without applying additional heat.

Keywords: graphene; graphane; corrugation; strain; desorption; DFT; bandgap



Citation: Boukhvalov, D.W.; Osipov, V.Y. Compression-Induced Dehydrogenation of Graphene: Insight from Simulations. *Hydrogen* **2023**, *4*, 1022–1034. <https://doi.org/10.3390/hydrogen4040059>

Received: 14 November 2023

Revised: 29 November 2023

Accepted: 6 December 2023

Published: 9 December 2023



Copyright: © 2023 by the authors. Licensee MDPI, Basel, Switzerland. This article is an open access article distributed under the terms and conditions of the Creative Commons Attribution (CC BY) license (<https://creativecommons.org/licenses/by/4.0/>).

1. Introduction

Since the first synthesis of single-wall carbon nanotubes [1], carbon nanosystems have been discussed as a prospective material for hydrogen storage [2]. Two possible mechanisms for hydrogen storage in graphene were proposed. The first is physical adsorption. Due to weak non-covalent bonds between H₂ molecules and carbon substrates, only selected porous structures with significant internal curvatures can hold significant amounts of hydrogen molecules [2]. On the contrary, the chemical adsorption of hydrogen atoms of honeycomb lattices can provide a C:H ratio equal to 1:1 [3]. Chemical adsorption of a hydrogen atom on a carbon atom belonging to a honeycomb lattice changes the hybridization of the carbon atoms from *sp*² to *sp*³. Also, it leads to visible distortion of the carbon flat in radii about 1 nm [4]. The availability of all atoms in graphene sheets for the chemical adsorption of hydrogen makes graphene an outstanding candidate for storing chemisorbed hydrogen. Pioneering works considered the hydrogenation of whole graphene demonstrate that an increase in hydrogen content leads to a decrease in the formation energy with a simultaneous turn reaction from endothermic to exothermic at a C:H ratio of about 2:1 [3]. Simulation of graphene's step-by-step hydrogenation and fluorination demonstrates a significant difference between these two processes [5]. In the case of fluorination, the formation of several stable intermediate CF_x structures was described theoretically. This result agrees with the experimental observation of various CF_x (where x= 0.12~0.90) structures.

On the contrary, step-by-step hydrogenation occurs smoothly without forming any stable intermediate CH_x structures [5]. Total hydrogenation of graphene and total dehydrogenation of graphane (graphene, 100% hydrogenated from both sides) as a result

of the annealing support this theoretical finding [6]. The described absence of stable intermediate CH_x structures makes hydrogenation of the graphene rather convenient. On the contrary, hydrogen extraction from graphane can be described as an all-or-nothing process. Annealing of the graphane leads to the fast removal of all hydrogen atoms from graphene. However, partial dehydrogenation of the graphane could be preferable in actual situations. Note that turning off the annealing mode does not lead to immediate cooling of the graphane and environment. Therefore, hydrogen release will continue further at a slower decaying pass. In addition, the combination of annealing at 350 °C required for the desorption of hydrogen [7]. Since molecular hydrogen is a highly combustible species, dehydrogenation of graphane by annealing arouses safety issues. Note that the annealing of hydrogenated graphene could also provide appearances of different perforations in the graphene membrane by forming volatile hydrocarbons (C_xH_y) molecules. The described process is a reversible reaction to the well-known healing of perforations in graphene membranes by annealing in the presence of carbohydrates observed in multiple experiments for different hydrocarbons [8,9]. These difficulties have yet to be discussed in the papers devoted to using graphene as hydrogen storage material.

Since the discovery of graphene in 2004 [10], hydrogen has become the ‘species of choice’ for the theoretical description of graphene’s chemical properties. Previous theoretical works described the adsorption of a single atom on graphene [11–13], configurations of a few hydrogen atoms on graphene [14,15], hydrogen adsorption on various defects [16], one-side hydrogenation [17], and the effect of the substrate [18,19]. Multiple works reported the results of systematic studies of hydrogen molecule decomposition on metal atoms and clusters on graphene surfaces [20–24]. Theoretical [25,26] and experimental works [26,27] demonstrated preferable hydrogenation or functionalization by other species of different corrugations of graphene flats, such as ripples and bends. These works demonstrate significant changes in the chemisorption energies from the shape and magnitude of local curvatures. The formation of graphene distortions was proposed as the method to facilitate the initial states of graphene hydrogenation [25,27–40]. The role of hydrogenation of the ripples’ top area on the protons’ permeation throughout graphene has been simulated in recent work [41,42]. However, the corrugation’s effect on chemisorbed hydrogen stability at a higher load of hydrogen (a C:H ratio below 10:1) and in graphane has not been discussed yet. A negative Poison ratio calculated for hydrogenated graphene [43] suggests that at higher levels of hydrogenation, the ripples’ shapes and magnitudes and the energetics of hydrogen chemical adsorption on ripples could be different.

Motivated by the lagoon in the knowledge about relationships between corrugations of graphene and the stability of hydrogen chemisorption, we performed the set of first-principles periodic DFT calculations. In this work, we report the results of systematic studies of non-hydrogenated and hydrogenated ripples of various shapes and magnitudes. We also reported the results of simulations of the initial stages of dehydrogenation of graphanes with multiple forms and magnitudes of the ripples. The stability of hydrogen clusters on the surface of ripples and the effect of these clusters on the migration barrier of protons throughout the graphene membrane is also reported in this paper.

2. Materials and Method

Theoretical modeling was carried out using the SIESTA pseudopotential code [44] employing the generalized gradient approximation (GGA-PBE) [45] for the exchange-correlation potential in a spin-polarized mode. The authors previously used this method to simulate graphene chemical properties and corrugations [3–5,16,18,25,41]. A complete optimization of the atomic positions was carried out. The electronic ground state was consistently found using norm-conserving pseudopotentials [46] for the cores with a double- ζ -plus polarization basis for the localized orbitals of carbon atoms and a double- ζ for hydrogen atoms. The cut-off radii for pseudopotentials of carbon and hydrogen were used 1.25 a.u. and 1.10 a.u, respectively. Note that the difference between the lattice parameters and energies of chemical processes on graphene-based systems calculated with

norm-conserving pseudopotentials is the same as calculated with the usage of more precise ultrasoft pseudopotentials (Refs. [3–5,16,18,25,41] vs. Refs. [27,31,42,47–50]). The forces and total energies were optimized with an accuracy of $0.04 \text{ eV } \text{Å}^{-1}$ and 1.0 meV/cell (or less than 0.02 meV/atom), respectively. Since we simulated only chemical adsorption of the hydrogen, special corrections for non-covalent (so-called van Der Waals bonds) were not used to describe covalent C—C and C—H bonds. For the protons (H^+) simulation, we generated pseudopotential with 0.05 e^- . The calculations were performed for the charged system with the charge $+0.995$. This method has been used before in Ref. [41]. Corrections of weak non-covalent bonds [51] were used for simulations of proton migration.

In the recent decade, the general standard approach to the simulation of graphene ripples was developed. The imitation of the ripples in graphene is the combination of in-plane compression of the graphene sheet with initial out-of-plane shift of several atoms in a relatively large supercell (usually containing more than 200 carbon atoms) and following optimization of only atomic structure with a fixed lattice constant [47–50]. In our work, we used the same approach to modeling the ripples in graphene and graphane.

3. Results and Discussions

3.1. Simulation of Non-Hydrogenated Ripples

The first step of our studies is the simulation of the ripples in pure graphene via a combination of in-plane compression and initial out-of-plane shift of a few atoms in the center of the supercell. For our simulations, we used a supercell of 240 carbon atoms in a graphene monolayer, shown in Figure 1. The in-plane lattice parameter of unstrained graphene is 2.462 Å . We decreased this parameter to 2.35, 2.30, 2.25, and 2.20 Å to imitate lattice compression. These changes in absolute values of lattice constant correspond with the relative decrease of lattice parameters at 4.5, 7.5, 8.4, and 11.3%. The results of the calculations show two different patterns in ripple formation. Note that expansion of the graphene membrane does not induce ripples and even decrease out-of-plane distortions caused by functionalization [52]. The slightest compression (at 4.5%) leads to the formation of ripples with hemisphere-like shapes, shown in Figure 1a. Increasing the compression leads to a transition toward the triangular shape of the ripples shown in Figure 1c,d. Numerical characterization of this triangular shape can be proposed as the presence of three directions where out-of-plane displacement of carbon atoms is larger than in other directions at the same distance from the top of the ripple. On the contrary, in the ripples of spherical shape, out-of-plane displacement of carbon atoms is equal in all directions at the same distance from the top of the ripple. These triangular-shaped ripples can also be discussed as a stack of the bends of graphene flats. Since the ripples of similar shape were also reported for slightly larger [47–50] and smaller supercells [52], the shape of observed ripples can be described as independent of supercell size. Note that the ratio of the height to width of the ripples used in previous works as a numerical characteristic of corrugations [16,42] cannot be applied for triangular-shaped ripples owing to the difficulties with recognizing the ripple's edges and therefore, the width of the ripples cannot be defined. The energy cost of forming simulated ripples is the difference between the total energy per carbon atom of a corrugated compressed and flat non-strained supercell. The energy cost of the ripple shown in Figure 1a is 125 meV per carbon atom. The formation of the ripples with morphologies is demonstrated in Figure 1b–d, which requires energies of 113 meV per carbon atom, 112 meV per carbon atom, and 143 meV per carbon atom, respectively. Thus, despite the minimal compression corresponding with the formation of the structure shown in Figure 1a, this structure is less energetically favorable than structures of different morphology shown in Figure 1c,d. The possible cause of the less favorable structure shown in Figure 1a is a mismatch between the symmetry of the hemisphere-shaped ripple and graphene lattice.

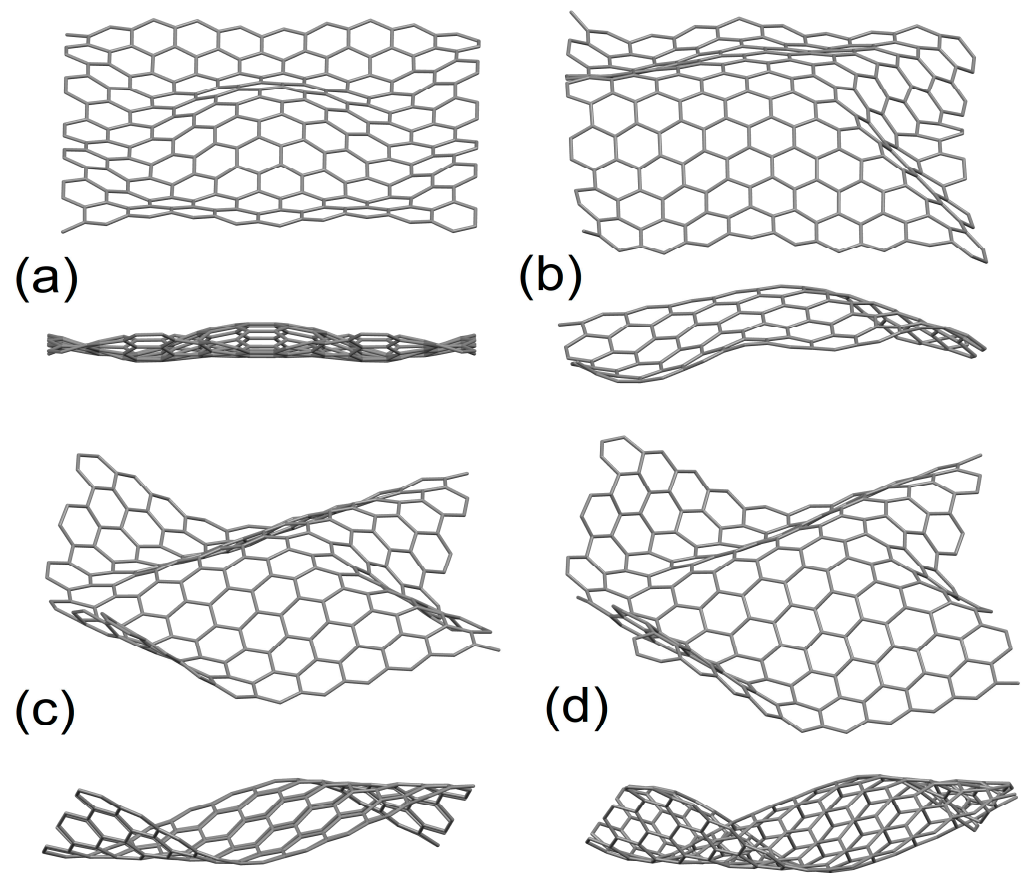


Figure 1. Optimized atomic structures of the ripples in graphene induced by uniaxial in-plane compression by 4.5% (a), 7.5% (b), 8.4% (c), and 11.3% (d) are shown from two different points of view.

To study the effect of the initial shape of the ripples on its morphology, we took structures shown in Figure 1a,d and changed the magnitudes of compression. An enhancement of the compression from 4.5% to 11.3% transforms the system shown in Figure 1a into the structure shown in Figure 2a. This structure is identical to the structure simulated for the same level of compression from the initial configuration shown in Figure 1d. Contrary, weakening of the compression from 11.3% to 4.5% leads to the transformation of the structure shown in Figure 1d to the configuration shown in Figure 2b, which have the shape similar to the system in Figure 1d with lower magnitude of out-of-plane distortions. The energy cost of the structure shown in Figure 2a is 145 meV per carbon atom, which is almost the same as the energy cost of the system formed under the same compression (11.3%) in Figure 1d. On the other hand, the formation of the structures with triangular morphology at minimal compression (4.5%) require relatively low energy (52 meV/ per carbon atom). Thus, since the formation of hemisphere-shaped ripples requires some peculiar starting conditions in simulations or fabrication of the scaffold with pre-adsorbed spherical nanoparticles [26,33], we can claim that the formation of hemisphere-like ripples (Figure 1a) is less “natural” than ripples of triangular shapes shown in Figures 1b–d and 2. To check the thermal stability of the ripples, we performed first-principles molecular dynamic simulation, within Nose thermostat for room temperature with the step of the simulation is 0.3 fs. Results of the calculations for 20 ns demonstrate the stability of the shape of the ripples corresponding with insignificant (0.02 Å) deviation of atoms from equilibrium positions.

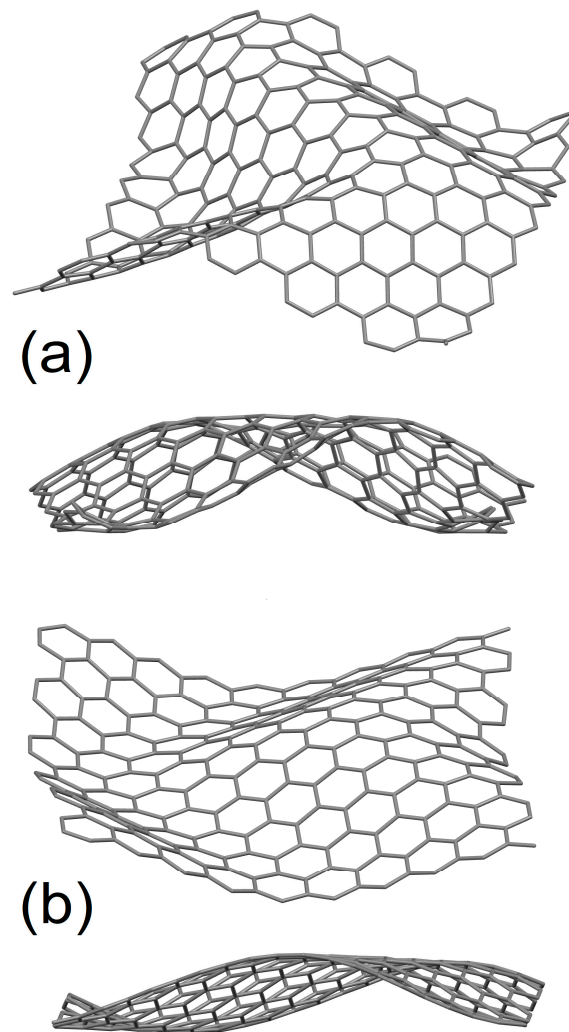


Figure 2. Optimized atomic structure of the ripple presented in Figure 1a after increasing in-plane compression up to 11.3% (a), and the ripple presented in Figure 1d after the decrease of in-plane compression to 4.5% (b). Both structures are shown from two different points of view.

The next step of our studies is to check the effect of corrugation on the electronic structure of corrugated graphene. Our previous work proposed the appearance of so-called “midgap states” on the Fermi level of corrugated graphene with hemisphere-shaped ripples [6]. The calculated electronic structure for the ripples shown in Figure 1 is presented in Figure 3a. The calculations results demonstrate the appearance of “midgap states” only for the ripples obtained for the smallest compression levels (4.5% and 7.3%). Note that the morphology of the ripple shown in Figure 1b (compression at 7.3%) can be described as containing signatures of hemisphere-shaped ripple shown in Figure 1a. Following increasing of in-plane compression of the graphene membrane with simultaneous formation of triangular-shaped graphene ripples leads to vanishing of “midgap states” and turn electronic structures to the similar with flat graphene. The main effect of different corrugation levels for triangular-shaped ripples is some changes in electronic structures in the areas from -2 eV to -0.5 eV and from 0.5 eV to 2 eV (see Figure 3a). These changes in electronic structure are caused by reciprocal disorientations of π -orbitals in strongly corrugated graphene.

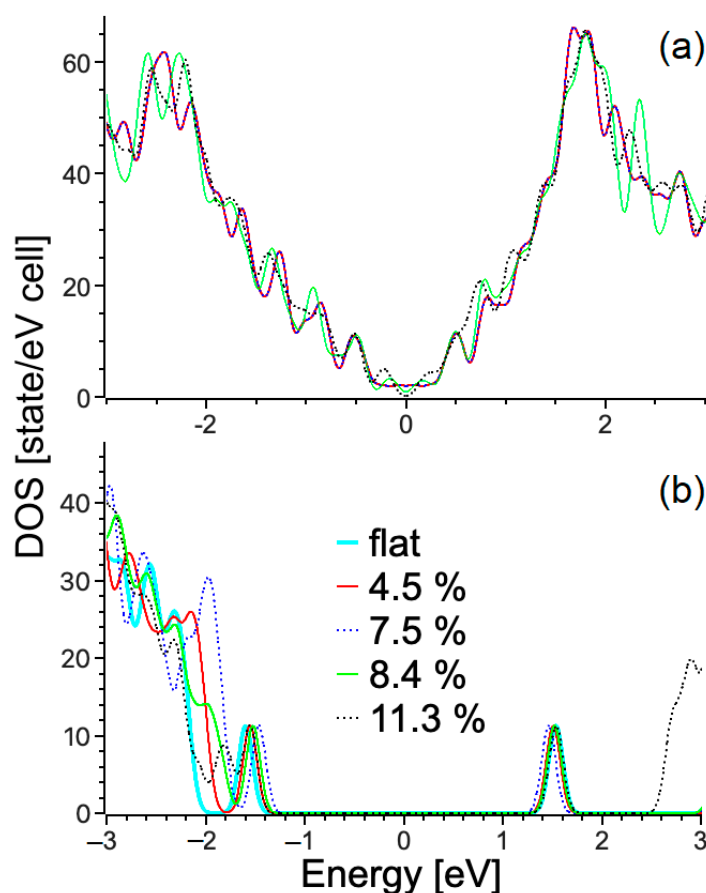


Figure 3. Total densities of states of corrugated graphene (a) and flat and corrugated graphene after desorption of four hydrogen atoms (b). The Fermi level is set as zero. Smearing with 0.1 eV of half-width on half-height was used in this plot.

3.2. Hydrogen Clusters on the Top of the Ripples

The next step of our work is the periodic DFT calculations of the adsorption of the pairs of hydrogen atoms on various ripples described in the previous section. First, we simulated the adsorption of the pairs of hydrogen atoms on an aromatic ring on the top of ripples shown in Figure 1a,d. Similar to the adsorption of monovalent species on flat graphene discussed in detail in Refs. [4,25], adsorption in ortho (nearest carbon sites) and para (adsorption on opposite sites of a hexagon) positions were considered. Optimized atomic structures corresponding with adsorption in ortho and para positions are shown in Figure 4a,c, respectively. To evaluate the stability of the hydrogen atoms on the carbon substrate, we calculate the energy cost of hydrogen desorption as H_2 molecules. The energy required for the desorption of hydrogen is defined as follows:

$$E_{\text{des}} = (E(\text{graphene} + 2n\text{H}) - [E(\text{graphene}) + nE(H_2)]) / 2n \quad (1)$$

where $E(\text{graphene} + 2n\text{H})$ is the energy of graphene substrate with adsorbed $2n$ hydrogen atoms, $E(\text{graphene})$ is the energy of corrugated graphene substrate considered in the discussed case, and $E(H_2)$ is the energy of the single hydrogen molecule in a gaseous phase. All total energies in this and the following equations are reported for optimized atomic structures. Positive values of E_{des} correspond with stable adsorption (desorption of hydrogen is an endothermic reaction).

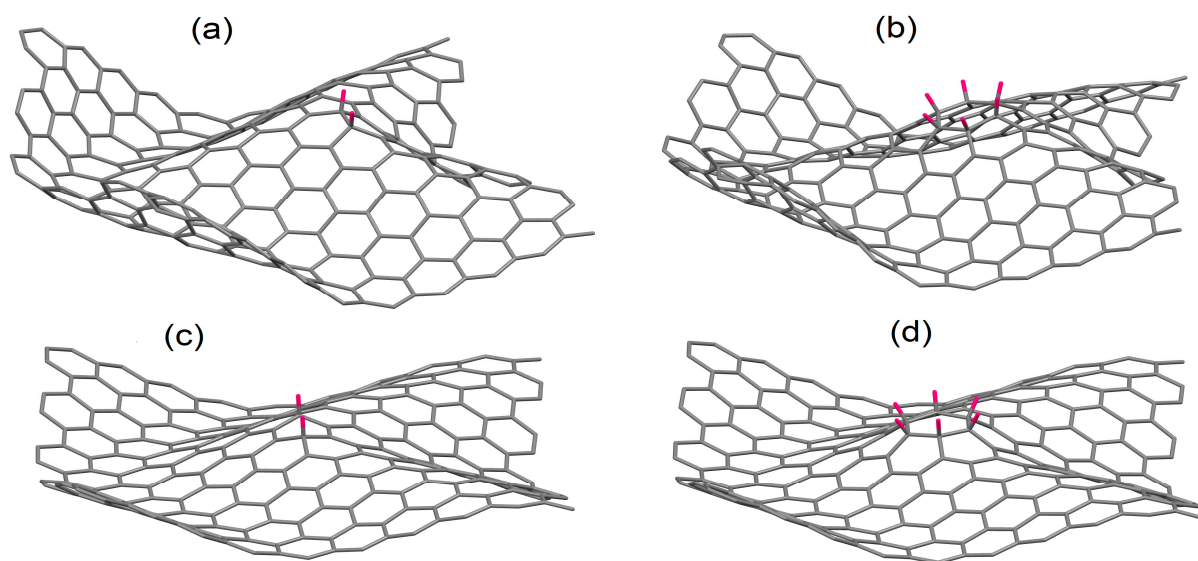


Figure 4. Optimized atomic structure of the ripples obtained by compression at 11.3% (a,b) and 4.5% (c,d) with a pair of hydrogen atoms in ortho (a) and para (c) positions and crown-like structure on the top of the ripples formed by six hydrogen atoms (b,d). Hydrogen atoms are shown in purple.

For ortho and para configurations, calculated desorption energies for hemisphere-like ripples are above 2 eV per hydrogen atom. Note that the adsorption of hydrogen atoms on hemisphere-shaped ripples shown in Figure 1a transforms the shape of these ripples to a shape similar to a more stable triangular-like shape shown in Figure 4c,d. On the other hand, for more energetically favorable triangle-shaped ripples, desorption of the hydrogen atoms is the exothermic process with the energy gain from reaction 0.1–0.18 eV per hydrogen atom.

Hydrogenation of all six carbon atoms in the aromatic ring on the top of the ripples with the formation of crown-like structures shown in Figure 4b,d corresponds with the same tendencies as for the pairs. Note that in previous theoretical works, where the favorability of the functionalization of the ripples was discussed, only less energetically favorable hemisphere-like ripples were considered [25]. In experimental works, extrinsic ripples in graphene flats were induced by the deposition of spherical nanoparticles on scaffolds and the deposition of graphene monolayer over these nanoparticles [26,33]. Thus, stable hydrogenation of the ripples proposed as the essential condition for permeating hydrogen protons through the graphene membrane by flipping, proposed in work by W. Xiong et al. [42], can be achieved only for some particular less energetically favorable local morphologies of graphene ripples.

The last step in this part of our studies is to check how the formation of crown-like structures on the top of the ripples (Figure 4b,d) affects the energy cost of the permeation of hydrogen protons through the graphene membrane. For this purpose, we placed the hydrogen proton in the center of a fully hydrogenated carbon ring and then performed optimization of atomic positions. The energy cost of permeation is defined as:

$$E_{\text{perm}} = (E(\text{substrate}) + E(\text{H}^+)) - E(\text{substrate} + \text{H}^+) \quad (2)$$

where $E(\text{substrate})$ is the total energies of structures shown in Figure 4b,d, $E(\text{H}^+)$ is the total energy of hydrogen proton, and $E(\text{substrate} + \text{H}^+)$ is the total energy of the considered system with the hydrogen proton located in the center of the hydrogenated ring [41,42]. Positive values of E_{perm} correspond with the endothermic process of the hydrogen proton permeation. Calculated values of E_{perm} are 1.4–2.0 eV per proton for various crown-like structures on the top of graphene ripples simulated for various magnitudes of in-plane compression. The proton permeation's energy cost values are more significant than those

calculated by the same method for non-hydrogenated flat graphene (about 1.4 eV per proton; see supplementary information for Ref. [41]). Thus, the flipping mechanism proposed for some ripples of unique shapes and magnitudes presented in work by W. Xiong et al. [42] can be discussed as the most probable mechanism of proton permeation through graphene. However, the local structure of hydrogenated ripples where proton flip occurs should be clarified according to discussions in this section. On the other hand, the unfavorability of a hydrogenation of the most energetically favorable ripples gives one a clue to the route for de-hydrogenation of graphene without annealing.

3.3. Hydrogen Desorption from Rippled Graphane

The final part of our studies is the periodic DFT calculations of the effect of a high hydrogenation level on the buckling of the graphene. First, we calculated a hundred percent two-sided hydrogenated graphene, also called graphane, and then performed a set of calculations similar to those described in Section 3.1. Calculated atomic structures corresponding with 4.5%, 7.5%, and 11.3% in-plane uniaxial compression of graphane are shown in Figure 5. One can see that compression of graphane at 4.5% does not lead to significant corrugation of the carbon flat (see Figure 5a). Further increase in compression of the graphane leads to the formation of the ripples (see Figure 5b,c). The cause of the observed difference between graphene and graphane is the hybridization of carbon atoms. In graphene, all carbon atoms have sp^2 hybridization with very rigid in-plane C=C bonds. Therefore, the only way to eliminate stress caused by compression is the formation of ripples where the lengths of carbon-carbon bonds remain almost unchanged.

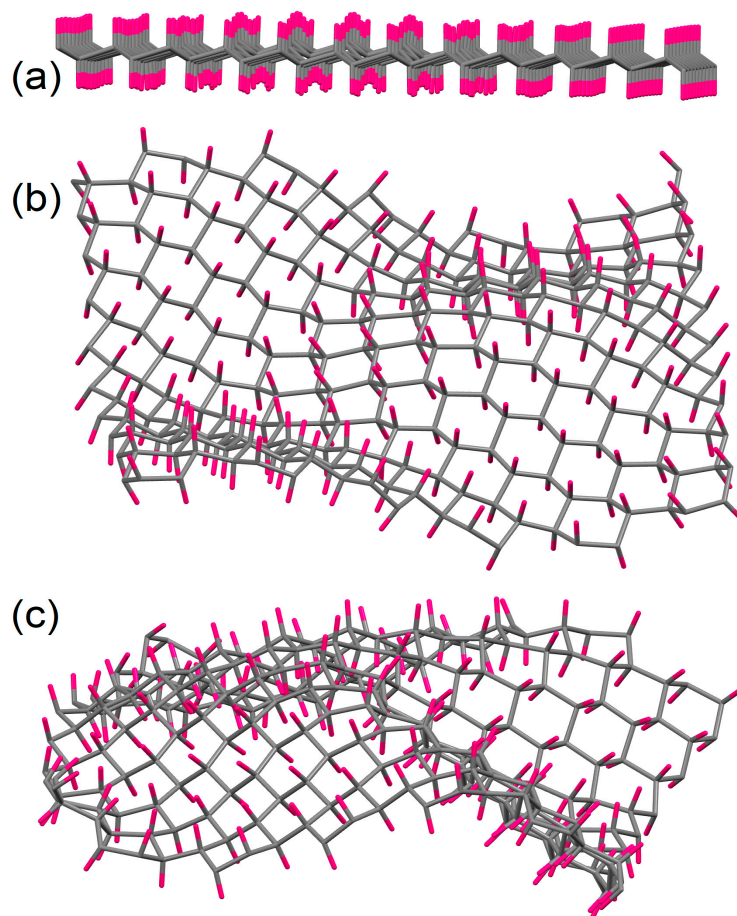


Figure 5. Optimized atomic structure of graphane uniaxial compressed at 4.5% (a), 7.5% (b), and 11.3% (c). Hydrogen atoms are shown in purple.

On the contrary, in graphane, all carbon atoms are in sp^3 hybridization. In other words, the atomic structure of graphane can be described as built from tetrahedra with hydrogen atoms on the tops. The stress caused by in-plane compression is first eliminated by the compression of these tetrahedra, leading to a simultaneous shift of the half carbon atoms up and the other half down. When at significant in-plane compressions, the limit of the compression of the tetrahedra is exceeded, and the formation of ripples with triangular shapes shown in Figure 5c can be observed. Note that incorporating sp^3 carbons in the top areas of stable (the most energetically favorable) ripples creates additional local distortions and, hence, destabilized hydrogen adsorption, as discussed in the previous section.

In the next step of our periodic DFT calculations, we calculated the binding energies for hydrogen on compressed and corrugated graphane using Equation (1). The total energies of non-hydrogenated graphane at the same level of in-plane compression are used as $E(\text{graphene})$. In the case of non-compressed and non-corrugated graphane, the binding energy is 0.42 eV per formula unit of graphane, which now contains carbon and hydrogen atoms and can be expressed as CH. Compression with the rippling of the graphane leads to a decrease in the binding energies of hydrogen to 0.39 eV per CH formula unit at a compression of 4.5%. Further compression of the graphane to 11.3% leads to a decrease in binding energy to 0.36 eV per CH formula unit. Note that a calculated tiny reduction in the binding energies is averaged over the whole supercell. Therefore, the energy cost of the desorption of a few hydrogen atoms could be much lower (see discussion below). On the other hand, the minor changes in the total energies per CH formula unit correspond with the absence of visible changes in the electronic structure of flat and corrugated graphane.

We performed periodic DFT calculations of step-by-step dehydrogenation of corrugated graphanes to verify the hypothesis proposed above. As a single desorption step, we consider simultaneous desorption of four nearest hydrogen atoms, two from one side and two from another (see Figure 6a,c). The described process corresponds with the formation of H_2 molecules from each side of the graphane. The following equation defines the energy cost of this process:

$$E_{\text{des}} = [(E(\text{graphene} + n\text{H}) - 2E(H_2)) - E(\text{graphene} + (n - 4)\text{H})]/4 \quad (3)$$

where $E(\text{graphene} + n\text{H})$ is the energy of graphene substrate with adsorbed n atoms of hydrogen, and $E(H_2)$ is the energy of hydrogen molecule in a gaseous phase. In the case of flat, non-compressed graphane, the energy cost of the four first steps of hydrogen desorption are 0.91–0.93 eV per hydrogen atom. This number explains why annealing at 350 °C is necessary to start the dehydrogenation of graphane [7]. The compression of graphane leads to a significant decrease in the desorption energies to the values of 0.33 eV per hydrogen atom for compression at 4.5% and 0.07 eV per hydrogen atom for compression at 11.3% (see data in Table 1). Note that in the case of minimal compression (4.5%), even desorption of four hydrogen atoms turns the almost planar structure shown in Figure 5a to a corrugated structure shown in Figure 6a. In the case of an already strongly corrugated structure (see Figure 5c) initial step of hydrogen desorption does not induce visible changes in morphology (see Figure 6c). Thus, compression of the graphane can lead to the start of spontaneous desorption of hydrogen even at room temperatures.

Table 1. The energies required for desorption of the four hydrogen atoms (two from each side) from graphane (Figure 6a,b) and semi-hydrogenated graphane (Figure 6c,d) at different levels of in-plane compression.

Lattice Compression, %	$E(\text{Graphane}), \text{eV/H}$	$E(\text{Semi-Hydrogenated}), \text{eV/H}$
Non-compressed flat graphane	0.93	0.42
4.5	0.33	0.35
7.5	0.24	0.32
8.4	0.11	0.30
11.3	0.07	0.29

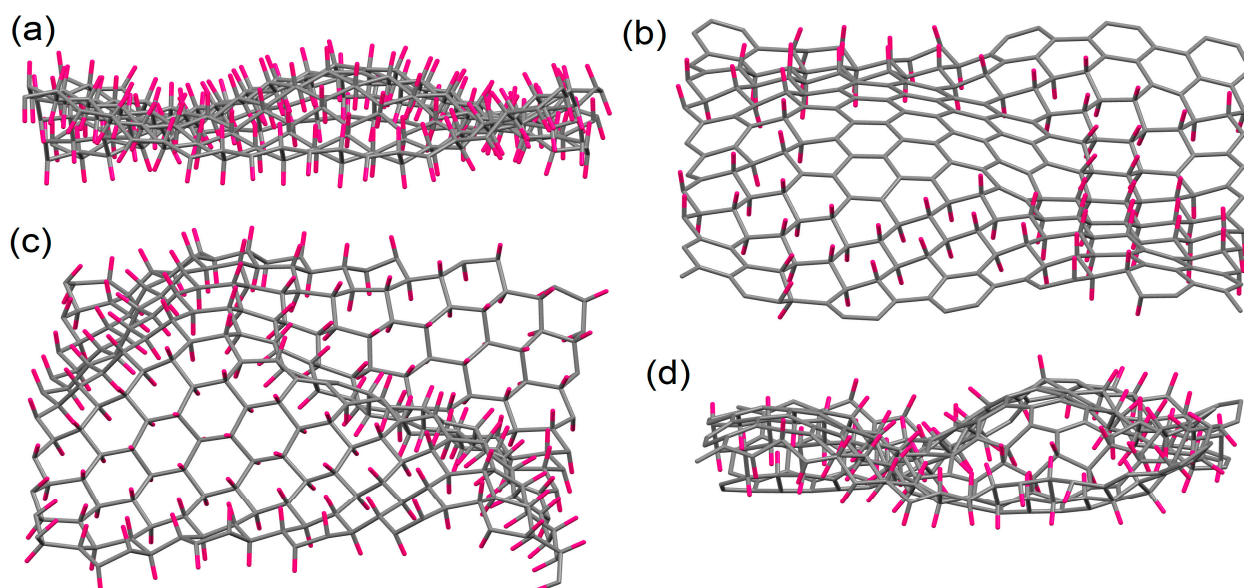


Figure 6. Optimized atomic structure of graphane uniaxially compressed at 4.5% (a,b), and 11.3% (c,d) after desorption of four (a,c) and half (b,d) of hydrogen atoms. Hydrogen atoms are shown in purple.

Desorption of two pairs of hydrogen atoms from corrugated graphane leads to the appearance of defect states inside the bandgap (see Figure 3b). These states are related to the formation of the clusters containing carbon atoms with sp^2 hybridization. The restoring of C=C bonds in the process of dehydration leads to re-appearance in the states related to bonding and antibonding π and π^* orbitals. Note that the position of described states inside the bandgap is the same for flat and corrugated graphanes. Since the value of the energy released by hydrogen in flat graphene is larger than in corrugated graphene, applying short-term corrugation with the following flattening of the graphane membrane can create and stabilize the states inside the bandgap. Thus, the corrugating of functionalized graphene membranes can also be used for gap engineering.

Further dehydration of flat graphane corresponds with energy costs of about 0.42 eV per hydrogen atom or 0.82 eV/mol for hydrogen molecules (see for details Ref. [5]). These energies are larger than the values of the enthalpy of water evaporation at room temperature (about 0.43 eV/mol [53]). Thus, hydrogenation and dehydrogenation processes will be in equilibrium at room temperature. Therefore, eliminating the corrugations should stop the process of dehydrogenation of graphane. The compression-induced corrugation of semi-hydrogenated graphanes shown in Figure 6b,d corresponds with desorption energies below 0.4 eV per hydrogen atom (0.35 eV per hydrogen atom for compression at 4.5% to 0.29 eV per hydrogen atom for compression at 11.3%). Thus, switching on and off compression of graphane will provide starting and quenching of the spontaneous dehydrogenation process.

4. Conclusions

The results of the calculations demonstrate the favorability of forming triangular-shaped ripples in corrugated graphene. Contrary to hemisphere-shaped ripples discussed in several previous works, hydrogenating these natural ripples by pairs and clusters of adatoms is energetically unfavorable. The appearance of so-called ‘midgap states’ on the Fermi level is also observed only for the ripples of hemisphere-like shapes. The formation of hydrogen clusters on the top areas of triangular-shaped ripples does not decrease the energy of proton permeation throughout the graphene membrane; thus, the flipping of adsorbed protons described in previous works can be currently considered the most probable mechanism of proton permeation.

The compression-induced corrugation of 100% hydrogenated graphene (graphane) leads to decreasing energy costs of the initial steps of hydrogen desorption from about

0.9 eV per desorbed hydrogen atom to 0.3 eV per desorbed hydrogen atom, even at the smallest values of considered compressions. This difference in the energy costs of hydrogen desorption from flat and corrugated graphene remains even after the desorption of half of the hydrogen atoms. Based on the results of our periodic DFT calculations, we propose inducing the corrugation of hydrogenated graphene as the route to the controllable release of hydrogen without annealing. Desorption of the pair of hydrogen atoms from each side of the graphene leads to the appearance of defect states inside the bandgap. The positions of these defect states are the same for flat and corrugated graphanes. Thus, partial dehydrogenation by corrugation can also be used for gap engineering in graphene and functionalized graphene-based systems.

Author Contributions: Investigation, Conceptualization, Software, Visualization, Writing —original draft and editing, Funding acquisition, D.W.B.; Validation, Data curation, Writing —review and editing, Funding acquisition, V.Y.O. All authors have read and agreed to the published version of the manuscript.

Funding: This research was funded by the Science Committee of the Ministry of Science and Higher Education of the Republic of Kazakhstan, grant number BR21881954. V.Y.O. acknowledges the support from Ioffe Institute, Russian Federation, (Project No. 0040-2019-0013).

Data Availability Statement: The data presented in this study are openly available in article.

Acknowledgments: The authors thank the reviewers of the article for their useful comments.

Conflicts of Interest: The authors declare no conflict of interest.

References

1. Tasis, D.; Tagmatarchis, N.; Bianco, A.; Prato, M. Chemistry of Carbon Nanotubes. *Chem. Rev.* **2006**, *106*, 1105–1136. [[CrossRef](#)]
2. Darkrim, F.L.; Malbrunot, P.; Tartaglia, G.P. Review of hydrogen storage by adsorption in carbon nanotubes. *Int. J. Hydr. Ener.* **2002**, *27*, 193–202. [[CrossRef](#)]
3. Boukhvalov, D.W.; Katsnelson, M.I.; Lichtenstein, A.I. Hydrogen on graphene: Electronic structure, total energy, structural distortion and magnetism from first-principles calculations. *Phys. Rev. B* **2008**, *77*, 035427. [[CrossRef](#)]
4. Boukhvalov, D.W.; Katsnelson, M.I. Chemical functionalization of graphene. *J. Phys. Cond. Matt.* **2009**, *21*, 344205. [[CrossRef](#)] [[PubMed](#)]
5. Boukhvalov, D.W. Absence of a stable atomic structure in fluorinated graphene. *Phys. Chem. Chem. Phys.* **2016**, *18*, 13287–13293. [[CrossRef](#)] [[PubMed](#)]
6. Elias, D.C.; Nair, R.R.; Mohiuddin, T.M.G.; Morozov, S.V.; Blake, P.; Halsall, M.P.; Ferrari, A.C.; Boukhvalov, D.W.; Katsnelson, M.I.; Geim, A.K.; et al. Control of Graphene's Properties by Reversible Hydrogenation: Evidence for Graphane. *Science* **2009**, *323*, 610–613. [[CrossRef](#)]
7. Morse, J.R.; Zugell, D.A.; Patterson, E.; Baldwin, J.W.; Willauer, H.D. Hydrogenated graphene: Important material properties regarding its application for hydrogen storage. *J. Power Sources* **2021**, *494*, 229734. [[CrossRef](#)]
8. Salehi, M.; Bastani, P.; Jamilpanah, L.; Madani, A.; Mohseni, S.M.; Shokri, B. Low defect and high electrical conductivity of graphene through plasma graphene healing treatment monitored with in situ optical emission spectroscopy. *Sci. Rep.* **2021**, *11*, 20334. [[CrossRef](#)]
9. Liu, L.; Qing, M.; Wang, Y.; Chen, S. Defects in Graphene: Generation, Healing, and Their Effects on the Properties of Graphene: A Review. *J. Mater. Sci. Tech.* **2015**, *31*, 599–606. [[CrossRef](#)]
10. Geim, A.K. Graphene: Status and Prospects. *Science* **2009**, *324*, 1530–1534. [[CrossRef](#)]
11. Ivanovskaya, V.V.; Zobelli, A.; Teillet-Billy, D.; Rougeau, N.; Sidis, V.; Briddon, P.R. Hydrogen adsorption on graphene: A first principles study. *Eur. Phys. J. B* **2010**, *76*, 481–486. [[CrossRef](#)]
12. Miura, Y.; Kasai, H.; Diño, W.A.; Nakanishi, H.; Sugimoto, T. Effective Pathway for Hydrogen Atom Adsorption on Graphene. *J. Phys. Soc. Jap.* **2003**, *72*, 995–997. [[CrossRef](#)]
13. Casolo, S.; Løvvik, O.M.; Martinazzo, R.; Tantardini, G.F. Understanding adsorption of hydrogen atoms on graphene. *J. Chem. Phys.* **2009**, *130*, 054704. [[CrossRef](#)] [[PubMed](#)]
14. Guan, Y.; Dutreix, C.; Gonzales-Herrero, H.; Ugeda, M.M.; Brihuega, I.; Katsnelson, M.I.; Yazyev, O.V.; Renard, V.T. Observation of Kekulé vortices induced in graphene by hydrogen adatoms. *arXiv* **2023**, arXiv:2307.10024.
15. Gallouze, M.; Kellou, A.; Drir, M. Adsorption isotherms of H₂ on defected graphene: DFT and Monte Carlo studies. *Int. J. Hydr. Ener.* **2016**, *41*, 5522–5530. [[CrossRef](#)]
16. Boukhvalov, D.W.; Katsnelson, M.I. Chemical functionalization of graphene with defects. *Nano Lett.* **2008**, *8*, 4373–4379. [[CrossRef](#)] [[PubMed](#)]

17. Pujari, B.P.; Gusarov, S.; Brett, M.; Kovalenko, A. Single-side-hydrogenated graphene: Density functional theory predictions. *Phys. Rev. B* **2011**, *84*, 041402. [[CrossRef](#)]
18. Boukhvalov, D.W. Modelling of epitaxial graphene functionalization. *Nanotechnology* **2011**, *22*, 055708. [[CrossRef](#)]
19. Verma, S.K.; Shaz, M.A.; Yadav, T.P. Enhanced hydrogen absorption and desorption properties of MgH₂ with graphene and vanadium disulfide. *Int. J. Hydr. Ener.* **2023**, *8*, 21383–21394. [[CrossRef](#)]
20. Shiraz, H.G.; Tavakoli, O. Investigation of graphene-based systems for hydrogen storage. *Renew. Sust. Ener. Rev.* **2017**, *74*, 104–109. [[CrossRef](#)]
21. Sigal, A.; Rojas, M.I.; Leiva, E.P.M. Interferents for hydrogen storage on a graphene sheet decorated with nickel: A DFT study. *Int. J. Hydr. Energ.* **2011**, *36*, 3537–3546. [[CrossRef](#)]
22. López-Corral, I.; Germán, E.; Juan, A.; Volpe, M.A.; Brizuela, G.P. DFT Study of Hydrogen Adsorption on Palladium Decorated Graphene. *J. Phys. Chem. C* **2011**, *115*, 4315–4323. [[CrossRef](#)]
23. Luhadiya, N.; Choyal, V.; Kundalwal, S.I.; Sahu, S.K. Investigation of unified impact of Ti adatom and N doping on hydrogen gas adsorption capabilities of defected graphene sheets. *J. Molec. Graph. Model.* **2023**, *119*, 108399. [[CrossRef](#)] [[PubMed](#)]
24. Jastrzębski, K.; Kula, P. Emerging Technology for a Green, Sustainable Energy-Promising Materials for Hydrogen Storage, from Nanotubes to Graphene—A Review. *Materials* **2021**, *14*, 2499. [[CrossRef](#)]
25. Boukhvalov, D.W.; Katsnelson, M.I. Enhancement of chemical activity in corrugated graphene. *J. Phys. Chem. C* **2009**, *113*, 14176–14178. [[CrossRef](#)]
26. Wu, Q.; Wu, Y.; Hao, Y.; Geng, J.; Charlton, M.; Chen, S.; Ren, Y.; Ji, H.; Li, H.; Boukhvalov, D.W.; et al. Selective surface functionalization at regions of high local curvature in graphene. *Chem. Comm.* **2013**, *49*, 677–679. [[CrossRef](#)]
27. Goler, S.; Coletti, C.; Tozzini, V.; Piazza, V.; Mashoff, T.; Beltram, F.; Pellegrini, V.; Heun, S. Influence of Graphene Curvature on Hydrogen Adsorption: Toward Hydrogen Storage Devices. *J. Phys. Chem. C* **2013**, *117*, 11506–11513. [[CrossRef](#)]
28. Kim, C.-E.; Lee, J.; Walsh, A.; Lordi, V.; Bahr, D.F. Role of ripples in altering the electronic and chemical properties of graphene. *J. Chem. Phys.* **2022**, *156*, 054708. [[CrossRef](#)]
29. Mangum, J.M.; Harerimanmetal, F.; Gikunda, M.N.; Thibado, P.M. Mechanisms of Spontaneous Curvature Inversion in Compressed Graphene Ripples for Energy Harvesting Applications via Molecular Dynamics Simulations. *Membranes* **2021**, *11*, 516. [[CrossRef](#)]
30. Hildebrand, M.; Abualnaja, F.; Makwana, Z.; Harrison, N.M. Strain Engineering of Adsorbate Self-Assembly on Graphene for Band Gap Tuning. *J. Phys. Chem. C* **2019**, *123*, 4475–4482. [[CrossRef](#)]
31. Lobzenko, I.; Baimova, J.; Krylova, K. Hydrogen on graphene with low amplitude ripples: First-principles calculations. *Chem. Phys.* **2020**, *530*, 110608. [[CrossRef](#)]
32. Baimova, J.A.; Krylova, K.A.; Lobzenko, I.P. Graphene crumpling as a method of hydrogen storage: Simulation results. *J. Micromech. Molec. Phys.* **2019**, *04*, 1950009. [[CrossRef](#)]
33. Gao, X.; Wang, Y.; Liu, X.; Chan, T.-L.; Irle, S.; Zhao, Y.; Zhang, S.B. Regioselectivity control of graphene functionalization by ripples. *Phys. Chem. Chem. Phys.* **2011**, *13*, 19449–19453. [[CrossRef](#)] [[PubMed](#)]
34. Li, Y.; Liu, X.; Chen, C.; Duchamp, J.; Huang, R.; Chung, T.-F.; Young, M.; Chalal, T.; Chen, Y.P.; Heflin, J.R.; et al. Differences in self-assembly of spherical C₆₀ and planar PTCDA on rippled graphene surfaces. *Carbon* **2019**, *145*, 549–555. [[CrossRef](#)]
35. Jain, V.; Kandasubramanian, B. Functionalized graphene materials for hydrogen storage. *J. Mater. Sci.* **2020**, *55*, 1865–1903. [[CrossRef](#)]
36. Ruffieux, P.; Gröning, O.; Biemann, M.; Mauron, P.; Schlapbach, L.; Gröning, P. Hydrogen adsorption on sp²-bonded carbon: Influence of the local curvature. *Phys. Rev. B* **2002**, *66*, 245416. [[CrossRef](#)]
37. Darvish Ganji, M.; Hosseini-Khah, S.M.; Amini-Tabar, Z. Theoretical insight into hydrogen adsorption onto graphene: A first-principles B3LYP-D3 study. *Phys. Chem. Chem. Phys.* **2015**, *17*, 2504–2511. [[CrossRef](#)]
38. 3Baitimbetova, B.A.; Ryabikin, Y.A.; Rakymetov, B.A.; Murzalinov, D.O.; Kantarbaeva, D.O.; Duamet, B.; Dmitriyeva, E.A.; Serikkanov, A.S.; Yelemessov, K. Paramagnetic Properties of Carbon Films. *Coatings* **2023**, *13*, 1484. [[CrossRef](#)]
39. Tozzini, V.; Pellegrini, V. Prospects for hydrogen storage in graphene. *Phys. Chem. Chem. Phys.* **2013**, *15*, 80–89. [[CrossRef](#)]
40. McKay, H.; Wales, D.J.; Jenkins, S.J.; Verges, J.A.; de Andres, P.L. Hydrogen on graphene under stress: Molecular dissociation and gap opening. *Phys. Rev. B* **2010**, *81*, 075425. [[CrossRef](#)]
41. Sun, P.Z.; Yang, Q.; Kuang, W.J.; Stebunov, Y.V.; Xiong, W.Q.; Yu, J.; Nair, R.R.; Katsnelson, M.I.; Yuan, S.J.; Grigorieva, I.V.; et al. Limits on gas impermeability of graphene. *Nature* **2020**, *579*, 229–232. [[CrossRef](#)]
42. Xiong, W.; Zhou, W.; Sun, P.; Yuan, S. Enhanced hydrogen-gas permeation through rippled graphene. *Phys. Rev. B* **2023**, *108*, 045408. [[CrossRef](#)]
43. Jiang, J.-W.; Chang, T.; Guo, X. Tunable negative Poisson's ratio in hydrogenated graphene. *Nanoscale* **2016**, *8*, 15948–15953. [[CrossRef](#)] [[PubMed](#)]
44. Soler, J.M.; Artacho, E.; Gale, J.D.; Garsia, A.; Junquera, J.; Orejon, P.; Sanchez-Portal, D. The SIESTA Method for Ab-Initio Order-N Materials Simulation. *J. Phys.: Condens. Matter.* **2002**, *14*, 2745. [[CrossRef](#)]
45. Perdew, J.P.; Burke, K.; Ernzerhof, M. Generalized Gradient Approximation Made Simple. *Phys. Rev. Lett.* **1996**, *77*, 3865. [[CrossRef](#)]
46. Troullier, O.N.; Martins, J.L. Efficient Pseudopotentials for Plane-Wave Calculations. *Phys. Rev. B* **1991**, *43*, 1993. [[CrossRef](#)]

47. Abualnaja, F.; Hildebrand, M.; Harrison, N.M. Ripples in isotropically compressed graphene. *Comput. Mater. Sci.* **2020**, *173*, 109422. [[CrossRef](#)]
48. Talla, J.A.; Ahmad, M.A. Structural and Electronic Properties of Rippled Graphene Monolayer: Density Functional Theory. *J. Electron. Mater.* **2022**, *51*, 2464–2474. [[CrossRef](#)]
49. Talla, J.A.; Msallam, Z.M. Influence of Induced Ripples on Optical Properties of Graphene: Density Functional Theory. *Russ. J. Inorg. Chem.* **2022**, *67* (Suppl 1), S52–S62. [[CrossRef](#)]
50. Talla, J.A.; Almahmoud, E.A.; Al-Khazleh, K.; Abu-Farsakh, H. Structural and Electronic Properties of Rippled Graphene with Different Orientations of Stone-Wales Defects: First-Principles Study. *Semiconductors* **2021**, *55*, 643–653. [[CrossRef](#)]
51. Dion, M.; Rydberg, H.; Schröder, E.; Langreth, D.C.; Lundqvist, B.I. Van der Waals density functional for general geometries. *Phys. Rev. Lett.* **2004**, *92*, 246401. [[CrossRef](#)]
52. Boukhvalov, D.W.; Son, Y.-W. Covalent functionalization of strained graphene. *Chem. Phys. Chem* **2012**, *13*, 1463–1469. [[CrossRef](#)]
53. Rumble, J. *CRC Handbook of Chemistry and Physics*, 102nd ed.; Taylor & Francis: Abingdon, UK, 2021.

Disclaimer/Publisher's Note: The statements, opinions and data contained in all publications are solely those of the individual author(s) and contributor(s) and not of MDPI and/or the editor(s). MDPI and/or the editor(s) disclaim responsibility for any injury to people or property resulting from any ideas, methods, instructions or products referred to in the content.